Comparison of independently calculated ab initio normal-mode displacements for the three C–H stretching vibrations of methanol along the internal rotation path

Li-Hong Xu [a], R.M. Lees [a], Jon T. Hougen [b,*], Joel M. Bowman [c], Xinchuan Huang [d], Stuart Carter [c]

[a] Center for Laser, Atomic, and Molecular Sciences (CLAMS), Department of Physics, University of New Brunswick, Saint John, NB E2L 4L5, Canada
[b] Sensor Science Division, National Institute of Standards and Technology, Gaithersburg, MD 20899-8441, USA
[c] Cherry L. Emerson Center for Scientific Computation, Department of Chemistry, Emory University, Atlanta, GA 30322, USA
[d] SETI Institute, 189 Bernardo Avenue, Suite #100, Mountain View, CA 94043, USA

ARTICLE INFO

ABSTRACT

Graphical displays of normal-mode coefficients from recent quantum chemical projected-frequency calculations are compared with analogous displays constructed after reexamination of results from more extensive higher-level calculations described earlier in the literature. Such comparisons confirm the facts that: (i) no geometrical phase is accumulated in these coefficients when the methyl top undergoes one complete internal-rotation revolution with respect to the frame, and (ii) some of the coefficients, when plotted against the internal rotation angle, exhibit near-cusp-like behavior at one or two angles. The connection between these graphical displays and the magnitude of "Jahn–Teller-like" and "Renner–Teller-like" torsion–vibration interaction terms in a previously reported model Hamiltonian, as well as the connection between the lack of geometric-phase accumulation in these graphs and the number of conical intersections enclosed by one full internal-rotation motion, are briefly discussed.

1. Introduction

In a recent publication [1], three of the authors presented graphical representations of the v_3, v_2, and v_9 methyl-top C–H stretching vibrations in methanol along the internal rotation path of methanol that were intended to shed light on possible subtleties arising in the normal-mode behavior. The frequencies along the path agreed well with earlier literature reports [2–4] (apart from some constant offsets). However, normal-mode plots for v_3, v_2, and v_9 expressed as coefficients along the internal rotation angle of the internal-coordinate local-mode stretching displacements of the three individual C–H bonds, as well as plots of Cartesian components of the hydrogen-atom displacement vectors for these three vibrations, showed two unexpected features. (i) No accumulation of geometric phase [5–11] was observed, i.e., all quantities returned to their original values after a complete 2π internal rotation of the methyl group was carried out, rather than transforming into their negatives (a possibility suggested in [2]). (ii) Various cusp-like features appeared in a number of the plots.

Since the calculations in [1] were carried out by using the commercial Gaussian suite of programs as a "black box," it seemed

important to try to verify independently the two surprising results mentioned above. Fortunately, a closely related, but much higher level, calculation using quite different software packages had been carried out seven years earlier [4] by the other three authors of the present paper. Because the analysis in [4] focused on other questions, and therefore did not include explicit tables or plots of eigenvector coefficients, we present in this work overlaid plots of numerical results for various corresponding quantities from the two studies. These plots agree remarkably closely with respect to both points (i) and (ii) above.

2. Calculation procedures

Although all relevant particulars are presented in Refs. [1,4], we briefly indicate below the differences in the calculations in those two works.

2.1. Potential surfaces

A potential surface was not actually determined in the calculations of [1]. Instead, energies and structures at 19 points on the steepest descent curve connecting the first-order saddle point at the top of the torsional barrier (point number 1) to the global

* Corresponding author. Fax: +1 301 869 5700.
E-mail address: jon.hougen@nist.gov (J.T. Hougen).

minimum at the bottom (point number 21) were calculated using the command [12] MP2 = Full/6-311+G(3df,2p) Geom = Check NO-SYMM IRC = (Stepsize = 8, MaxPoints = 25, Forward, RCFC, Very-Tight) in the Gaussian 03 suite of programs [13]. With this command, the "geometry is optimized at each point along the reaction path such that the segment of the reaction path between any two adjacent points is described by an arc of a circle, and so that the gradients at the end points of the arc are tangent to the path" [14]. The IRC path is computed in mass-weighted internal coordinates (default [14]).

In [4] on the other hand, energies at nearly 20 000 appropriately chosen points on the potential surface were calculated using MOLPRO 2002.6 "at the coupled cluster singles, doubles, and non-iterative triples correction CCSD(T) level together with a correlation-consistent polarized valence triple-ζ basis augmented with diffuse functions (aug-cc-pVTZ)." These points were then fit to a potential energy surface using 3338 coefficients in a procedure [15] designed to insure that the surface has the correct symmetry for all possible large-amplitude vibrational excursions, i.e., designed to insure that the surface is invariant to all permutation-inversion operations.

2.2. Projected vibrational frequencies and vibrational displacements along the internal rotation path

In [1], vibrational frequencies and normal modes were calculated at each of the 19 points along the steepest descent path by feeding the geometries from Section 2.1 into G03, with the command MP2 = Full/6-311+G(3df,2p) Freq = (Projected, HPModes). With this command, for a point on a mass-weighted reaction path (IRC), Gaussian computes the projected frequencies for vibrations perpendicular to the path. For the projection, the gradient is used to compute the tangent to the path [14]. For points 1 and 21, i.e., at the stationary points at the top and bottom of the potential curve, the second part of the command was altered to read Freq = (HPModes) GEOM = Check.

In [4], the potential surface from Section 2.1 was used in the Reaction Path version of the variational code MULTIMODE (denoted MM-RPH) to determine vibrational frequencies and normal modes. In addition to determining normal modes and frequencies on the path, the authors of [4] also reported "configuration interaction" calculations of the coupled anharmonic energies and wave functions.

A point to note is that the projected-frequency calculations in [1] were carried out only from one maximum of the torsional potential curve to the adjacent forward minimum, i.e., over a 60° increase in torsional angle, whereas the calculations in [4] were carried out over a 180° change in torsional angle, i.e., over an interval that takes a given methyl hydrogen atom from its original eclipsed position in the molecular plane of symmetry to a staggered position in the molecular plane of symmetry. As a consequence, when making eigenvector plots the authors in [1] were forced to piece together six segments, with suitable reflections and overall sign changes as explained in Section 4.1 of [1], in order to obtain one complete eigenvector plot covering a full 360° change in internal rotation angle. In contrast, the data from the calculations in [4] needed to be pieced together only once to cover a full 360° change in internal rotation angle. The latter procedure is obviously much less susceptible to the introduction of "operator errors."

3. Overlaid plots of numerical results from [1,4]

3.1. Vibrational frequencies for v_3, v_2 and v_9

We discuss the three methyl stretching vibrations in the order v_3, v_2 and v_9, since v_3 (of symmetry A′ in the C_s point group of

methanol) corresponds reasonably closely [1] to the A_1 symmetric CH stretch in the related C_{3v} molecule CH_3F, while v_2 and v_9 (of symmetry A′ and A″, respectively, in the C_s point group) correspond [1] to the two components of the doubly degenerate E asymmetric CH stretch in CH_3F.

Fig. 1 shows as solid black curves the vibrational frequencies for v_3, v_2 and v_9 determined in [1] for a 60° change in torsional angle. Superimposed on these solid black curves are red dotted curves showing the vibrational frequencies determined in [4] after an appropriate energy offset, i.e., after a 60 cm^{-1} increment for v_3, and a 72 cm^{-1} increment for both v_2 and v_9. These increments are about 2% of the frequencies of the v_3, v_2 and v_9 vibrations, and almost certainly arise from the difference in calculation level between [1,4]. The relative changes in the much smaller energy difference from torsional maximum to minimum (i.e., the relative shifts in the zero-point contribution to the internal-rotation barrier heights from these three small-amplitude vibrations) are less than 6%.

The conclusion of importance for the present work is that the calculations in [1,4] give very similar patterns of variation for the CH stretching vibrational frequencies in methanol along the internal rotation path.

3.2. Normal modes for v_3, v_2 and v_9

Normal modes Q can conveniently be expressed numerically as a set of coefficients multiplying some set of specified vibrational
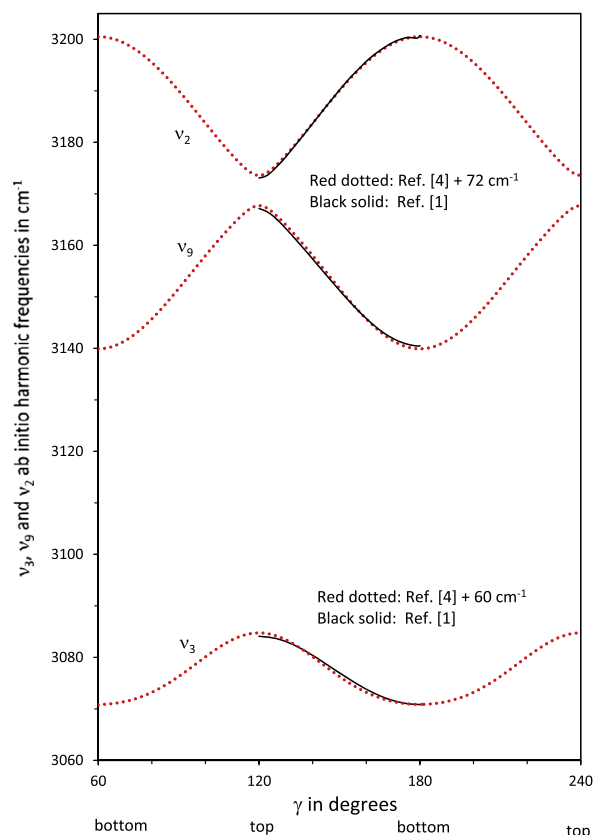
Fig. 1. Overlay of vibrational frequencies for the C–H stretching modes v_3, v_2, and v_9 as a function of the internal rotation coordinate in methanol. Solid black curves – as determined in [1]. Dotted red curves – as determined in [4], after a shift upward of 60 cm^{-1} for v_3, and a shift upward of 72 cm^{-1} for v_2 and v_9. Apart from the shift in absolute energies, the curves from [1,4] agree extremely well with each other. (For interpretation of the references to color in this figure legend, the reader is referred to the web version of this article.)

basis functions S. This set of coefficients is frequently called the L matrix, as defined by the equation

$$S = L(\gamma)Q, \tag{1}$$

where the traditional constant L matrix of Eq. (2) in Appendix VIII of Ref. [16] is taken to be a function of the torsional angle γ in the present work.

The vibrational basis functions S are often taken to be internal coordinates consisting of bond lengths, bond angles, and dihedral angles, since for these coordinates the six degrees of freedom corresponding to overall translation and overall rotation of the molecule have been removed. However, the basis functions S in Eq. (1) can also be taken to be Cartesian displacements of the individual atoms in the molecule along the principal rotational axis directions, which lend themselves well to visual display of the vibrational modes. It is the three components of the displacement vector for one of the methyl hydrogen atoms during a complete 360° internal rotation of the methyl group that are displayed for each of the ν_3, ν_2 and ν_9 vibrations in the nine panels of Fig. 2.

The three panels of the first column of Fig. 2 thus show the torsional variation of the z, x, and y components of the ν_3 vibrational

displacement vector of hydrogen number 5 (in the numbering of [1]) in the principal axis system. The solid black curves show plots of the numerical results from [1], the dotted red curves show plots of the numerical results from [4]. It is immediately evident that: (i) the solid and dotted curves in column 1 are almost identical, (ii) both sets of curves return to their original values and slopes after the 2π internal rotation (i.e., there is no non-zero accumulation of geometric phase), and (iii) all curves are either even or odd with respect to reflection at $\gamma = 60°$ and $\gamma = 240°$, as required by the symmetry of the problem when H_5 is in the molecular symmetry plane [1]. As explained in [1], symmetry requires that curves for the displacement vectors of hydrogen atoms 4 and 6 are identical to those here, except for a shift of torsional angles along the abscissa by ±120°.

The three panels of the second column of Fig. 2 show the z, x, and y components in the rotational principal axis system of hydrogen number 5 for ν_2. The solid black curves show plots of the numerical results from [1], the dotted red curves show plots of the numerical results from [4]. The two sets of curves again exhibit good numerical agreement, no geometric phase, and reflection symmetry (points (i), (ii), and (iii) in the previous paragraph), but
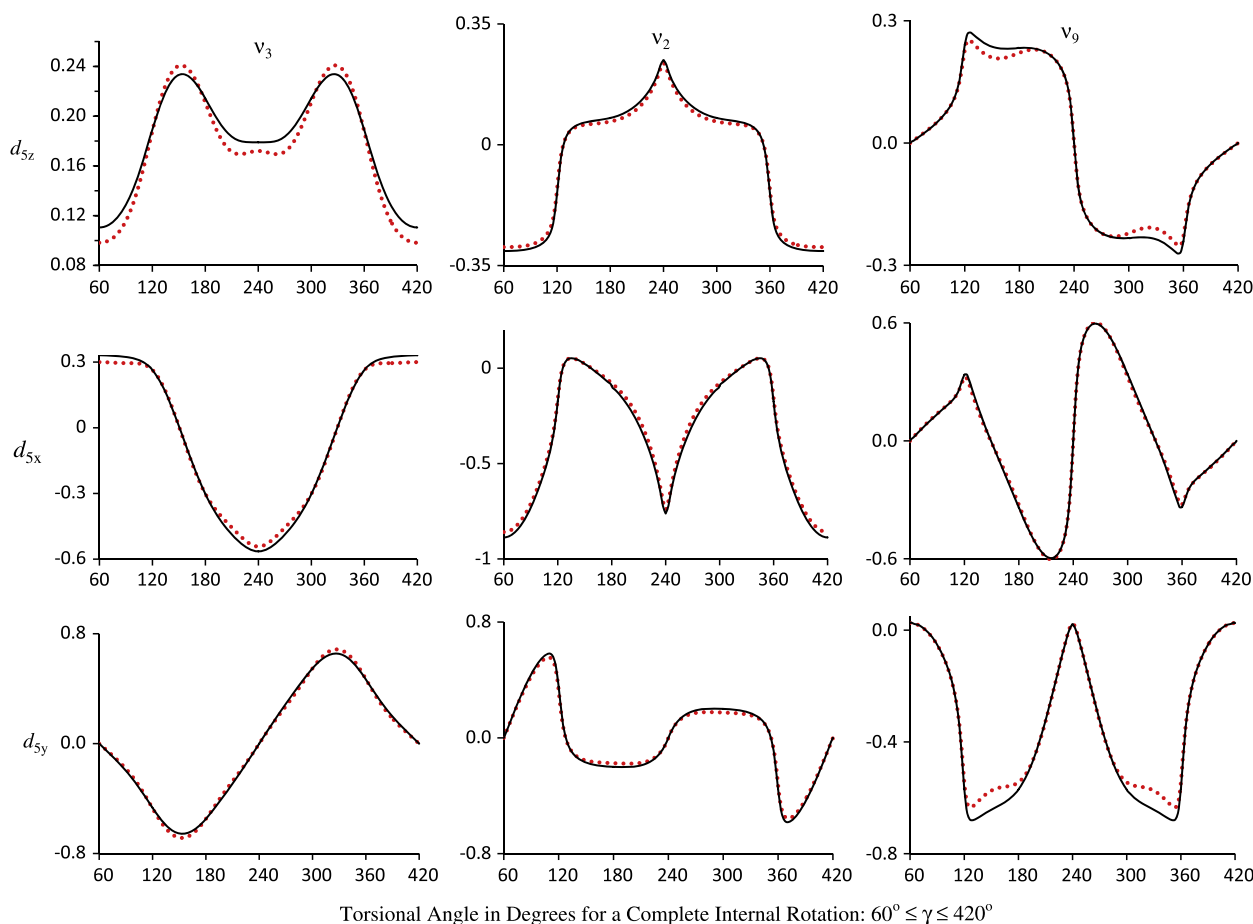
Fig. 2. Overlay of Cartesian components of the vibrational displacement vectors, as a function of the internal rotation angle, for one of the methyl hydrogen atoms involved in the C–H stretching modes ν_3, ν_2, and ν_9 of methanol. Solid black curves – displacements shown for H_5 in Fig. 5 of [1]. Dotted red curves – displacements determined from results obtained in [4]. Note that values for the internal rotation angle and for the overall phase factors have been changed to agree with those in [1]. Thus, displacements for H_3 of [4] between $\tau = 0°$ and 360° are plotted after adding 60° to their τ values. Furthermore, to obtain the full 360° internal rotation interval, displacements from [4] between $\tau = 0°$ and 180° had to be extended, essentially by reflecting them about $\tau = 180°$. The reflected parts of the four displacements that vanish at $\tau = 180°$, i.e., d_{3y} of ν_3, ν_2, and d_{3z}, d_{3x} of ν_9, had to be multiplied by -1 to maintain continuity of their first derivatives. Finally, d_{3x} of ν_3 and d_{3z} and d_{3y} of ν_2 and ν_9 had to be multiplied by -1 over their full 360° range to make their overall signs agree with the signs in [1]. The last sign change above (or lack thereof) is not completely random. It can be shown to be consistent with: (i) a C_{2z} rotation of Cartesian coordinate systems between Fig. 1 of [1] and Fig. 1 of [4], (ii) a change in the positive sense of the internal rotation angle between [1,4], and (iii) a change in the arbitrary overall phase factor for the ν_2 displacements. (For interpretation of the references to color in this figure legend, the reader is referred to the web version of this article.)

this time the first two panels of the second column also show rather sharp cusp-like features at $\gamma = 240°$. (See Section 6.2 of [1] for a brief discussion of the fact that these are not true cusps.)

The three panels of the third column of Fig. 2 show the z, x, and y components of hydrogen 5 for v_9. Remarks similar to those for the second column hold for this third column as well, except that the agreement between solid and dotted curves is not quite as good, and the cusp-like features are slightly less sharp. As expected [1] for this A″ vibration, points with even reflection symmetry in the first two columns become points with odd reflection symmetry in column three, and vice versa.

Fig. 2 illustrates the main point of this paper, since it shows clearly that two quite different calculations of the methyl hydrogen displacement vectors along the internal rotation path for the v_3, v_2 and v_9 vibrations in methanol give nearly identical numerical results. Fig. 2 thus provides independent confirmation of some of the conclusions in [1]. (Readers who wish to view the normal modes under discussion here as arrows along the three CH bonds, as depicted at the top of Fig. 8 of [9], can determine the signed lengths of these arrows for v_2 and v_9, respectively, from the two columns of the matrix in Eq. (26) of [1], using the function $\beta(\gamma)$ given in Eq. (10) there. Graphical representations of these arrow lengths for v_3, v_2, and v_9, are shown in Figs. 2 and 11 of [1].)

4. Calculation of other values of the Jahn–Teller and Renner–Teller parameters k_1 and k_2

According to the three-parameter model developed in Section 5 of [1], the v_2 and v_9 normal mode coefficients of internal coordinates, as well as the corresponding v_2 and v_9 Cartesian displacements, will transform into their negatives (e.g., Fig. 8 of [9]) or into themselves (e.g., Fig. 2 above) after one full internal rotation motion, depending on whether the ratio $|k_1/k_2|$ is greater or smaller than unity, where k_1 and k_2 are coefficients of the Jahn–Teller-like and Renner–Teller-like torsion–vibration interaction terms, respectively. (This qualitative statement is quantified by the function $\beta(\gamma)$ defined in Eq. (10) of [1].) It is thus of interest to compare the values of k_1 and k_2 presented in [1] (and given in Eq. (25) there) with those determined from the vibrational frequencies calculated in [4], as well as from two "hybrid" sets of mixed theoretical and

experimental frequencies, to see if ratios of $|k_1/k_2|$ greater than unity will arise.

As it happens, the values given in [1] were determined from a set of four equations in three unknowns by discarding one of the equations. Here, we keep all four equations giving calculated vibrational frequencies v at the top and bottom of the torsional barrier for the A′ (v_2) vibration and the A″ (v_9) vibration, i.e.,

$$v_{top}(A') = (k_E/m)^{1/2}[1 + (1/2)(k_1 + k_2)/k_E]$$
$$v_{top}(A'') = (k_E/m)^{1/2}[1 - (1/2)(k_1 + k_2)/k_E]$$
$$v_{bottom}(A') = (k_E/m)^{1/2}[1 + (1/2)(-k_1 + k_2)/k_E]$$
$$v_{bottom}(A'') = (k_E/m)^{1/2}[1 - (1/2)(-k_1 + k_2)/k_E], \qquad (2)$$

and then use a least-squares procedure to determine the three parameters on the right. These parameters consist of ratios involving: (i) the force constant k_E for the doubly degenerate E vibration corresponding to an unsplit $v_2 \oplus v_9$ mode, (ii) k_1 corresponding to the coefficient of the Jahn–Teller-like interaction term in Eq. (5a) of [1], and (iii) k_2 corresponding to the coefficient of the Renner–Teller-like interaction term in Eq. (5b) of [1]. The least-squares equations for this case are extremely simple, and lead to

$$(k_E/m)^{1/2} \equiv v_E = (1/4)\{[v_{top}(A') + v_{top}(A'')] + [v_{bottom}(A') + v_{bottom}(A'')]\}$$
$$v_E(k_1/k_E) = (1/2)\{[v_{top}(A') - v_{top}(A'')] - [v_{bottom}(A') - v_{bottom}(A'')]\}$$
$$v_E(k_2/k_E) = (1/2)\{[v_{top}(A') - v_{top}(A'')] + [v_{bottom}(A') - v_{bottom}(A'')]\}. \qquad (3)$$

Table 1 presents values of these ratios determined from four different sets of input v's, i.e., from the Gaussian calculations in [1], or from the MOLPRO calculations in [4], or from two "hybrid" sets of vibrational frequencies formed by combining the theoretical v_2 and v_9 frequencies given in [1] for the top of the barrier with experimental v_2 and v_9 frequencies (or term values) available at the bottom of the torsional well. The latter were taken from either high-resolution [17] or low-resolution [18] studies, and then adjusted by a shift chosen to make the average of each pair of experimental frequencies at the bottom of the well equal to the average at the bottom of the theoretical frequencies from [1]. This adjustment is required by the three-parameter model in [1], which assumes that the $(1/2)(v_2 + v_9)$ average is nearly the same at the top and bottom of the barrier, so that it can be represented by the single parameter $v_E \equiv (k_E/m)^{1/2}$ in Eq. (2).

It is clear from Table 1 that the $|k_1/k_2|$ ratio is less than unity for all four cases, i.e., none of these model calculations predicts [1] a geometric phase change of -1 for the adiabatically calculated CH stretching vibrational coefficients or displacements (i.e., for quantities calculated at different fixed values of the internal rotation angle) after going once around the internal rotation motion.

Turning now to the question of torsional splittings in the CH stretching fundamentals, we recall that the three-parameter model in [1] predicts that the torsional splittings in v_2 and v_9 will be inverted, whatever the value of the ratio $|k_1/k_2|$ is, provided only that the torsional splitting is small compared to the $|v_2 - v_9|$ vibrational frequency difference. Table 2 lists torsional splittings for v_2 and v_9 predicted using k_1 and k_2 values from Table 1. It was hoped that hybrid results using experimental information at the bottom of the barrier would significantly improve the prediction of these A/E splittings, but this did not turn out to be the case. It is not clear at present if this is caused: (i) by the simplicity of the three-parameter model (whose range of applicability has not been extensively tested), (ii) by inaccurate ab initio vibrational frequencies at the top of the barrier (where experimental adjustment is not feasible), or (iii) by some unsuspected perturbation(s) affecting the experimentally determined A/E splittings (e.g., it is difficult to understand why the best agreement with experiment comes from the hybrid data set containing the low-resolution frequencies).

Table 1
Values[a] of various ratios of the parameters k_E, k_1, and k_2 from Eq. (2), as determined by Eq. (3) from the theoretical data in [1,4], or from a hybrid mix of theoretical and experimental data (see Section 4).

	Ref. [1][b]	Ref. [4][c]	Hybrid Hi-Res[d]	Hybrid Low-Res[e]
$v_{top}(A')$	3173.0735	3101.5817	3173.0735	3173.0735
$v_{top}(A'')$	3167.1614	3095.7112	3167.1614	3167.1614
$v_{bottom}(A')$	3200.7185	3128.5020	3191.5209	3185.1109
$v_{bottom}(A'')$	3140.5033	3067.9155	3149.7009	3156.1109
$v_E = (k_E/m)^{1/2}$	3170.364	3098.428	3170.364	3170.364
$v_E k_1/k_E$	−27.152	−27.358	−17.954	−11.544
$v_E k_2/k_E$	33.064	33.229	23.866	17.456
$|k_1/k_2|$	0.821	0.823	0.752	0.661

[a] All quantities are in cm⁻¹, except for $|k_1/k_2|$, which is unitless.
[b] Theoretical vibrational frequencies v taken from Table 5 of [12] and used in [1], and four ratios of parameters determined from them.
[c] Theoretical vibrational frequencies v from the harmonic calculations in [4], and ratios of parameters determined from them.
[d] Ratios of parameters determined from Eq. (3) by using theoretical vibrational frequencies from [1] at the top of the barrier, but using vibrational term values (including the $v_t = 0$ torsional zero-point energy) at the bottom, as determined from high-resolution experimental frequencies [17]. The A and E components of v_2 (or v_9) in Ref. [17] were averaged using a weight factor of 1:2. Both averages were then shifted up by 58.6042 cm⁻¹ (see text).
[e] Ratios of parameters determined by using theoretical vibrational frequencies from [1] at the top of the barrier, but using low-resolution experimental frequencies [18] at the bottom, after shifting them up by 186.1109 cm⁻¹ (see text).

Table 2

Torsional splittings $E(A) - E(E)$ for v_2 and v_9, as determined from Eq. (34) of [1] and values of the parameters k_E, k_1, and k_2 in the various columns of Table 1.

	Expt[a]	Ref. [1][b]	Ref. [4][c]	Hybrid Hi-Res[d]	Hybrid Low-Res[e]
v_2	3.26	4.22 (29%)	4.22 (29%)	4.07 (25%)	3.86 (18%)
v_9	5.48	4.90 (11%)	4.90 (11%)	5.05 (8%)	5.26 (4%)

[a] High-resolution experimental results from Ref. [17].

[b] Predicted from k_E, k_1, and k_2 in column 2 of Table 1, i.e., from parameters based on the ab initio results in Ref. [1], together with a calculated (but not experimentally observable) ground state torsional splitting of 9.12 cm^{-1}. (Note that because of a notation change, the expression $(k_1 + k_2)$ in Eq. (34) of [1] must be replaced by $(-k_1 + k_2)$ before substituting values from Table 1.) Values in parentheses in this and other columns to the right give the percent difference from experiment.

[c] From column 3 of Table 1, based on the ab initio results in Ref. [4].

[d] From column 4 of Table 1, based on ab initio results in Ref. [1] and high-resolution experiments in Ref. [17].

[e] From column 5 of Table 1, based on ab initio results in Ref. [1] and low-resolution experiments in Ref. [18].

It is also of interest to continue the search for quantum chemical calculations that give vibrational displacement plots similar to those in Fig. 2, but which exhibit a -1 phase change after one complete internal rotation. Such calculations could be performed for methanol at either a higher or lower level of sophistication, or for some related molecule like CH$_3$SH. Eq. (3) shows that $|k_1/k_2| > 1$ when the frequency ordering of the $v_2(A')$ and $v_9(A'')$ modes is different at the bottom and top of the internal rotation potential barrier. Since $|k_1/k_2| > 1$ gives rise [1] to the -1 phase change sought in this paragraph, calculation of symmetry-labeled vibrational modes at the C$_s$ global-minimum and the C$_s$ saddle point of methanol provides a simple diagnostic for identifying quantum chemical calculations that will yield the -1 phase change when a projected-frequency calculation is carried out. (See Ref. [19] for a more general discussion of the relation between the -1 phase change and the change in A' and A'' ordering of vibrational modes at the top and bottom of the barrier, which does not rely on the simple three-parameter model leading to Eq. (3).)

Looking at this in more detail from the point of view of quantum chemistry calculations, it seems reasonable to assume that the experimental value of $v_2(A') - v_9(A'') = 42$ cm^{-1} [17] is now well established. It also seems reasonable to assume that any future theoretical calculations will not deviate too much from the present theoretical value including anharmonic corrections, namely $v_2(A') - v_9(A'') = 25$ cm^{-1} [4]. (Note that the harmonic vibrational frequencies plotted in Fig. 2 give $v_2(A') - v_9(A'') = 60$ cm^{-1} [1,4].) In particular, even though the theoretical anharmonic value is lower than experiment by 17 cm^{-1}, it seems unlikely that future calculations will disagree with the experimentally determined order of $v_2(A') > v_9(A'')$ for methanol in its equilibrium conformation.

The situation at the top of the barrier is less clear, however, since the theoretical harmonic value $v_2(A') - v_9(A'') = 6$ cm^{-1} is much closer to zero, and no experimental check is possible. It is not difficult to imagine that some future change in basis set or computational procedure could change the sign of this small difference, which would then immediately lead to $|k_1/k_2| > 1$ and a -1 phase change for the displacement vectors after one complete internal rotation motion. In this connection, it is intriguing to note that exploratory anharmonic calculations carried out using the potential surface of [4], indicate that the $v_2(A') > v_9(A'')$ ordering might be reversed at the saddle point, since the anharmonicity of the $v_2(A')$ mode at the saddle point is larger than that of the $v_9(A'')$ mode. Details of this anharmonic vibrational analysis, which will be repeated using a newer potential surface, will be reported in due course.

On another topic, it would also be of interest to examine quantum chemical plots like those in Fig. 2 (as well as any associated algebraic models) for the methyl rocks and methyl bends in CH$_3$-OH, where the experimental results seem to indicate both inverted and regular torsional splittings occur. The rocks and bends are not nearly as isolated from other fundamental modes as the high frequency stretches are, however, so that both the theoretical and experimental interpretations for these modes may be strongly affected by interactions with neighboring fundamental modes not included in the simple two-mode model of [1].

5. Conical intersections

The occurrence of -1 phase changes in real wavefunctions of the high-frequency "fast" coordinates after having gone once around a closed loop in the low-frequency "slow" coordinates is intimately connected to the presence of a conical intersection somewhere inside the closed loop. While it is not the purpose of this short paper to review the vast literature that has emerged on this topic during the past half century, a few brief remarks are nevertheless of interest.

Zwanziger and Grant pointed out [10] that in the E electronic and e vibrational system, with the well-known conical intersection at the origin of the vibrational coordinates, one can find three additional conical intersections in the vicinity of the origin. Furthermore, depending on zero-point energies, the correct closed-loop trajectory in vibrational space will enclose some given set of these conical intersections. When an odd number of conical intersections is enclosed, one expects a phase change of -1. When an even number is enclosed, one expects a phase change of $+1$. Following up on this, Perry and Dawadi [20] are in the process of reexamining the vibrational potential surface for the torsion-vibration problem in methanol. They indeed find [20] three additional conical intersections near the central one. Full investigation of this situation, leading hopefully to a theoretically justified count of exactly how many conical intersections are enclosed by the "correct" closed-loop circuit in this problem, may well give an explanation for why the normal mode calculations in [1,4] in fact produce no change in geometric phase after one complete internal rotation, instead of the often supposed change of -1.

Conical intersections are known to lead to faster than normal dynamics in the vibronic problem. Hamm and Stock have recently [21] extended this vibronic thinking to the purely vibrational case of fast (OH stretch) and slow (hydrogen-bonding) modes. Their ideas should also be directly applicable to the present problem of fast (CH stretches) and slow (torsion) vibrational motions.

References

[1] Li-Hong Xu, J.T. Hougen, R.M. Lees, J. Mol. Spectrosc. 293–294 (2013) 38–59.
[2] B. Fehrensen, D. Luckhaus, M. Quack, M. Willeke, T.R. Rizzo, J. Chem. Phys. 119 (2003) 5534–5544.
[3] E.L. Sibert III, J. Castillo-Chará, J. Chem. Phys. 122 (2005) 194306-1–194306-11.
[4] J.M. Bowman, X. Huang, N.C. Handy, S. Carter, J. Phys. Chem. A 111 (2007) 7317–7321.
[5] H.C. Longuet-Higgins, U. Öpik, M.H.L. Pryce, R.A. Sack, Proc. Roy. Soc. 244A (1958) 1–16.
[6] H.C. Longuet-Higgins, Adv. Spec. 2 (1961) 429–472.
[7] G. Herzberg, Electronic Spectra and Electronic Structure of Polyatomic Molecules, Van Nostrand, 1966.
[8] M.V. Berry, Proc. Roc. Soc. 392A (1984) 45–57.
[9] D.S. Perry, J. Mol. Spectrosc. 257 (2009) 1–10.
[10] J.W. Zwanziger, E.R. Grant, J. Chem. Phys. 87 (1987) 2954–2964.
[11] J. Schön, H. Köppel, J. Chem. Phys. 103 (1995) 9292–9303.

[12] Li-Hong Xu, J.T. Hougen, J.M. Fisher, R.M. Lees, J. Mol. Spectrosc. 260 (2010) 88–104.
[13] Certain commercial products are identified in this paper in order to specify adequately the experimental or theoretical procedures. In no case does such identification imply recommendation or endorsement by the National Institute of Standards and Technology, nor does it imply that the products are necessarily the best available for the purpose.
[14] A. Frisch, M.J. Frisch, G.W. Trucks, Gaussian 03 User's Reference, 2003, pp. 88 and 126.
[15] X. Huang, B.J. Braams, J.M. Bowman, J. Chem. Phys. 122 (2005) 044308-1–044308-12.
[16] E.B. Wilson, J.C. Decius, P.C. Cross, Molecular Vibrations, McGraw-Hill, 1955.
[17] X. Wang, D.S. Perry, J. Chem. Phys. 109 (1998) 10795–10805.
[18] A. Serrallach, R. Meyer, Hs.H. Günthard, J. Mol. Spectrosc. 52 (1974) 94–129.
[19] J.T. Hougen, J. Mol. Spectrosc. 181 (1997) 287–296.
[20] D.S. Perry, M. Dawadi, Private Communication, 2013.
[21] P. Hamm, G. Stock, Phys. Rev. Lett. 109 (2012) 173201-1–173201-5.